Two-dimensional Crystallization of *Escherichia coli*-expressed Bacteriorhodopsin and Its D96N Variant: High Resolution Structural Studies in Projection

Alok K. Mitra,* Larry J. W. Miercke, George J. Turner, Richard F. Shand,‡ Mary C. Betlach, and Robert M. Stroud

Department of Biochemistry and Biophysics, University of California, San Francisco, California 94143-0448; ‡Department of Biological Sciences, Northern Arizona University, Flagstaff, Arizona 86011 USA

ABSTRACT Highly ordered two-dimensional (2-D) crystals of *Escherichia coli*-expressed bacteriorhodopsin analog (e-bR) and its D96N variant (e-D96N) reconstituted in *Halobacterium halobium* lipids have been obtained by starting with the opsin protein purified in the denaturing detergent sodium dodecyl sulfate. These crystals embedded in glucose show electron diffraction in projection to better than 3.0 Å at room temperature. This is the first instance that expressed bR or a variant has been crystallized in 2-D arrays showing such high order. The crystal lattice is homologous to that in wild-type bR (w-bR) in purple membranes (PM) and permit high resolution analyses of the structure of the functionally impaired D96N variant. The e-bR crystal is isomorphous to that in PM with an overall averaged fractional change of 12.7% (26–3.6-Å resolution) in the projection structure factors. The projection difference Fourier map e-bR-PM at 3.6-Å resolution indicates small conformational changes equivalent to movement of $\sim<7$ C-atoms distributed within and in the neighborhood of the protein envelope. This result shows that relative to w-bR there are no global structural rearrangements in e-bR at this 3.6 Å resolution level. The e-D96N crystal is isomorphous to the e-bR crystal with a smaller (9.2%) overall averaged fractional change in the structure factors. The significant structural differences between e-D96N and e-bR are concentrated at high resolution (5–3.6 Å); however, these changes are small as quantified from the 3.6 Å resolution e-D96N-e-bR Fourier difference map. The difference map showed no statistically significant peaks or valleys within 5 Å in projection from the site of D96 substitution on helix C. Elsewhere within the protein envelope the integrated measure of peaks or valleys was $<\sim3$ C-atom equivalents. Thus, our results show that for the isosteric substitution of Asp^{96} by Asn, the molecular conformation of bR in its ground state is essentially unaltered. Therefore, the known effect of D96N on the slowed M_{412} decay is not due to ground-state structural perturbations.

INTRODUCTION

Bacteriorhodopsin (bR) is a light-activated proton pump organized in a highly ordered two-dimensional (2D) P3 lattice in the specialized PM patches of *Halobacterium halobium* where it is the sole protein (Stoeckenius and Bogomolni, 1982). BR contains an all-*trans* retinylidene chromophore covalently linked to the ϵ-amino group of Lys^{216} through a protonated Schiff base. Upon illumination, isomerization of the chromophore from the all-*trans* to 13-*cis* (Mathies et al., 1988) takes place which initiates a photocycle involving at least six intermediates (Lozier et al., 1975, 1992). The net result is a vectorial translocation of 1.1 ± 0.2 protons/bR molecule/photocycle from the interior to the exterior of the cell (Grzsiek and Dencher, 1986). Extensive spectroscopic and functional studies on site-directed mutants have identified which amino acids interact most strongly with the chromophore and affect the proton pump (reviewed in Khorana, 1988; Trissl, 1990; Mathies et al., 1991; Lanyi, 1992; Rothschild, 1992; Oesterhelt et al., 1992). Until 1990 all site-directed studies had been carried out on bacterioopsin analogs expressed in *Escherichia coli* (Karnik et al., 1987; Shand et al., 1991). More recently site-directed mutants in bR-deficient *H. halobium* strain have been expressed and studied (Needleman et al., 1991; Turner et al., 1993). Based on electron crystallographic analyses of PM, Hayward and Stroud (1981), by addition of small regions of images determined the projected structure of PM at 3.7-Å resolution, and recently a three-dimensional structural model of bR at 3.5-Å in-plane resolution and ~10-Å resolution perpendicular to the membrane plane has been determined from electron cryomicroscopy (Henderson et al., 1990). These studies have greatly advanced our understanding toward a molecular model of the proton pump in bR.

The two key steps in the photocycle of bR are the deprotonation of the SB during the photointermediate L → M transition and reprotonation of SB in the photointermediate M → N transition. Recent studies on the single-site replacements of buried aspartates have revealed that Asp^{85} and Asp^{96} are intimately involved in these transitions. It is suggested that a carboxylate group with unusually low pK_a ~2.5 (Rothschild et al., 1981) assigned to Asp^{85} (Braiman et al., 1988) accepts the proton from the SB during L → M transition (Braiman et al., 1988), while Asp^{96} with its elevated pK_a (~10) (Metz et al., 1992) is involved in proton uptake

Received for publication 28 December 1992 and in final form 12 May 1993.

*Present address: Department of Cell and Molecular Biology, The Scripps Research Institute, 10666 North Torrey Pines Rd., La Jolla, CA 92037.

Abbreviations used: bR, bacteriorhodopsin; PM, purple membrane; SB, Schiff base; e-bO, *E. coli*-expressed β-gal-bacterioopsin fusion protein; e-bR, retinylated e-bO; e-D96N, Asp^{96}-Asn e-bR variant; SDS, sodium dodecyl sulfate; CHAPSO, 3-[(3-cholamidopropyl)dimethylammonio]-2-hydroxy-1-propanesulfonate; NG, nonyl-β-D-glucopyranoside; OG, octyl-β-D-glucopyranoside; DTAC, dodecyl trimethyl ammonium chloride; CHAPS, 3-[(3-cholamidopropyl)dimethylammonio]-1-propanesulfonate.

0006-3495/93/09/1295/12 $2.00

and SB reprotonation (Braiman et al., 1988; Gerwert et al., 1989; Holz et al., 1989; Otto et al., 1989; Thorgeirsson et al., 1991) and is deprotonated during the M → N transition (Bousche et al., 1991). The formation of the photo-excited M_{412} intermediate in the Asp^{85}-Asn variant is inhibited resulting in complete extinction of proton pumping (Braiman et al., 1988; Miercke et al., 1991). Interestingly, recent studies on this variant from *H. halobium*-expressed material shows that in the pH range 6–12 the protein exists as three spectroscopic species in equilibrium which are homologs of M, N, and O photo-intermediates (Turner et al., 1993). The D96N variant shows reduced proton pumping due to slowed decay of the M_{412} intermediate (Holz et al., 1989). Another aspartate, Asp^{212} has been suggested to play a more indirect role acting as one of the participants of the proton acceptor complex (Needleman et al., 1991).

In functionally impaired variants the effect exerted by single amino acid substitution on the photocycle and chromophore environment can also be modulated by structural rearrangements. Therefore, it is necessary to characterize any change in the structure in addition to function to separate localized chemical/electrostatic effect of mutation from possible large-scale structural alterations relayed to the rest of the protein. In this work we have used electron diffraction as a sensitive high resolution assay (Mitra and Stroud, 1990) to probe the structure in the functionally impaired D96N variant. Starting with e-bO expressed in large quantities (Shand et al., 1991) and purified to homogeneity (Miercke et al., 1991) we developed a method for obtaining large two-dimensional (2-D) crystals of e-bR that diffracted to high resolution and have lattices very similar to that in PM. Using an analogous protocol, we prepared 2-D crystals of the e-D96N variant. Here we compare in projection the ground state structures of e-bR and wild-type bR in PM and the structures of e-D96N and e-bR by difference Fourier analyses.

MATERIALS AND METHODS

Materials

Buffers used were the following: 0.1% (w/v) sodium dodecyl sulfate (SDS; Bio-Rad, Richmond, CA), 100 mM sodium acetate, pH 6.0 (Buffer A); 50 mM NG (CalBiochem, San Diego, CA), 5 mM sodium acetate, 4 mM sodium azide, pH 5.0 (Buffer B); 18 mM NG, 5 mM sodium acetate, 4 mM sodium azide, pH 5.0 (Buffer C); 10 mM sodium acetate, 4 mM sodium azide, 16 mM CHAPSO (Boehringer Mannheim Biochemicals, Indianapolis, IN), pH 5.0 (Buffer D); Buffer D, 0.5 M NaCl (Buffer E); 100 mM sodium acetate, 4 mM sodium azide, pH 5.0 (Buffer F); 30 mM sodium phosphate, pH 6.0 (Buffer G); 100 mM potassium phosphate, 6 mM OG (Pfanstiel Labs., Waukegan, IL), 200 μM DTAC (Eastman Kodak Co., Rochester, NY), pH 5.2 (Buffer H); 10 mM sodium acetate, 4 mM sodium azide, pH 5.0 (Buffer I); 10 mM sodium acetate, pH 5.0 (Buffer J); Triton X-100 (Pierce, Rockford, IL), DMPC (Avanti Polar lipids, Birmingham, AL), CHAPS (Fluka, Ronkonkoma, NY), all-*trans* retinal (Sigma Chemical Co., St. Louis, MO). D-Glucose and the salts were reagent grade.

Purification and 2-D crystallization of *E. coli*-expressed protein

Large-scale e-bO expression (17 mgs/liter) was carried out according to Shand et al. (1991). Retinylation and purification to homogeneity of wild-type fusion protein e-bR and e-D96N variant were carried out as described (Miercke et al. 1991) with modifications. All-*trans* retinal incorporation was carried out overnight upon mixing, by volume, 200 parts of 0.3–0.4 mg/ml of protein in Buffer A, 40 parts of 4% DMPC/4% CHAPS in water, 80 parts of water and 2 molar equivalents (retinal to protein) retinal. The reaction mixture was 0.2-μm filtered, concentrated 4–5-fold with high pressure filtration, YM-30 membrane (Amicon Inc., Beverly, MA), and applied (3–5-ml sample/tube) on top of a 6.5% (w/v) sucrose in Buffer B with a 22% w/v cushion and spun in a VTi50 rotor at 45,000 rpm, 4°C for 40 h. Protein at the sucrose-cushion interphase was directly applied to "Red-A" dye-ligand matrix (Millipore Corp., Bedford, MA) which had been equilibrated with Buffer C. The matrix was washed with 10 column volumes of Buffer D, and the protein eluted with Buffer E to produce pure bR monomer in CHAPSO which contained <0.05 mol of lipid phosphorous/mol of bR as determined from lipid-phosphate analysis (Miercke et al., 1989).

Reconstitution and 2-D crystallization of the retinylated fusion-protein in polar lipids extracted from PM or from whole cells of *H. halobium* (Kates et al., 1982) was performed using the protocol we developed (Miercke et al., 1991) and described in more detail here in the form of a flow chart in Fig. 1. Reconstitution/crystallization was carried out by dialysis in dark at 4°C for 2–5 weeks using Spectropore 6 (25-kDa molecular cut-off) membranes. All handling of detergent-solubilized protein samples was done under dim red light. Detergent exchange and protein concentration were carried out in the dark at 4°C using high pressure filtration and YM-30 membranes. Crystallized samples of e-bR and e-D96N in buffer F were stored at 4°C.

Expression in and purification of D96N membranes from *H. halobium*

The bacterio-opsin gene containing the D96N mutation was subcloned from the *E. coli* expression vector pβgbop (Shand et al., 1991) into the *E. coli/H. halobium* shuttle vector pUBP2 (Blaseio and Pfeifer, 1990). Subsequently, the latter construct was transformed into the BR-deficient *H. halobium* strain L33 (Wagner et al., 1983) by the method of Cline et al. (1989). *H. halobium*-D96N growth and harvesting was as described in Turner et al. (1993). The membranes, after removing sucrose by centrifugation, were resuspended in buffer G. In order to obtain large (~5-μm diameter) crystals for electron diffraction studies, these membrane patches (~0.8-μm average diameter) were subsequently fused (henceforth referred to as h-D96N samples) in buffer H using the protocol of Henderson et al. (1990).

The concentration of bR was assayed by optical absorbance using a value of 54,000 cm^{-1} M^{-1} for the molar extinction coefficient at the visible absorption maximum of detergent-solubilized samples and using a value of 63,000 for membrane-reconstituted samples. Optical absorbances were measured in a Shimadzu UV-160 spectrophotometer.

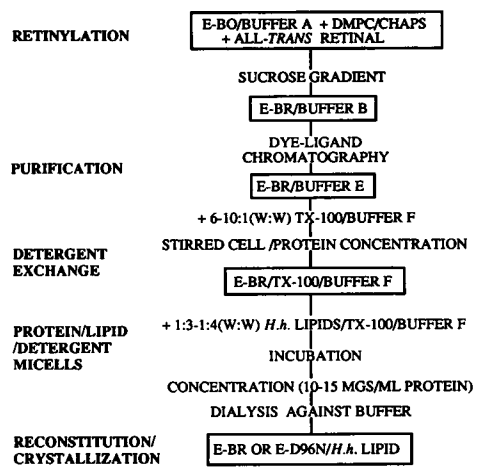

FIGURE 1 A flow diagram of the protocol for obtaining large (~5-μm average diameter) 2-D crystals of *E. coli*-expressed wild-type and bR variants.

Specimen preparation and electron diffraction

Crystalline specimens were applied, typically 4 μl, on a 400-mesh copper grid covered with a thin carbon film. This film was floated off a freshly cleaved mica sheet on to a clean double-distilled water surface and then gently lowered onto the grids. The carbon-coated grids were air-dried, and the carbon films were aged for at least 2–3 days to make them hydrophobic. Prior to sample application the carbon film was washed with several drops of 100% ethanol (Quantum Chemical Corp., Tuscola, IL) and then air-dried.

e-bR crystals suspended at ~10 μM protein concentration in buffer I containing 0.7% (w/v) glucose was used for specimen preparation. e-D96N crystals were washed with a 50 × volume of buffer J to remove azide and then suspended at ~10 μM protein concentration in buffer J containing 0.7% (w/v) glucose for specimen preparation. After letting the sample settle for 2 min, excess liquid was drawn off slowly by touching the edge of the grid with the tip of a cut Whatman filter paper and the grid was air-dried.

H-D96N samples in buffer H were applied at ~30 μM protein concentration and allowed to settle for 30 s to 1 min. Next the grid was gently tapped on a Whatman filter paper to remove most of the liquid, and then 5 μl of 0.7% glucose solution in water was applied and allowed to settle for 45 s. Finally, after removing the excess liquid with a cut tip of Whatman filter paper, the grid was air-dried.

Grids, thus prepared, were examined within 24 h or were stored at −20°C until used.

Electron diffraction from glucose-embedded samples was carried out at room temperature at 100 kV in an EM400 electron microscope (Phillips Electronic Instruments, Eindhoven, The Netherlands) using a 30-μm second condenser aperture, 0.2-μm spot size, and a total dose of ~0.4 $e/Å^2$. The procedure for collecting low dose electron diffraction patterns was as described by Mitra and Stroud (1990). During each session at the microscope, diffraction patterns from oriented gold crystals (Ted Pella Inc., Redding, CA) and calibration films with known electron exposures were recorded at the given microscope setting. The [200] 2.04-Å reflection from oriented gold crystals was used as a diffraction calibration standard. The recording film used was Kodak 4496 (S0–163G) (Eastman Kodak Co., Rochester, NY) which was developed for 16 min in fresh undiluted Kodak D19 developer at 20°C.

Data acquisition and analyses

Diffraction patterns and films for calibrating optical density to electrons were digitized on a flatbed microdensitometer (model 1010 M, Perkin-Elmer Corp., Norwalk, CT) whose output was filtered by a 4302 dual 242B/Octave band-pass filter (Ithaco, Ithaca, NY) to damp high frequency noise. The aperture and step size for digitizing the diffraction patterns was 10 μm, while these were 30 μm for digitizing the dose-calibration films.

Reconstituted e-bR and e-D96N sheets sometimes consisted of a single surface lattice but usually had two and up to four superimposed P3 lattices each of which were twinned, in general, to different extents. In order to visually assess the resolution, specimen tilt and number of overlapping lattices each digitized diffraction pattern was displayed on a Parallax 1280 display processor (Parallax Corp., Sunnyvale, CA) after 3×3 nearest-neighbor pixel averaging. Using the positions of the maxima of strong reflections, the least-squares refined [01] and [10] lattice vectors for all contributing lattices were obtained. The digitized pattern was smoothed and optical densities converted to electrons using the data from calibration films relating optical density to electron exposure (Katre et al., 1984). Next, starting with the predicted positions of all the reflections in the lattice that showed most intense spots (major lattice), a "matched filter" algorithm (Katre et al., 1984) was employed to accurately locate the centers and evaluate the background-corrected intensities. In this process whenever the center of a reflection spot for this "major" lattice was within twice the average spot radius of spot/s belonging to the other "minor" lattice/s it was not considered for intensity measurement. Such rejections usually constituted <10% of the total list of reflections for a given pattern. Four diffraction patterns from nominally untilted e-bR crystals and five from nominally untilted e-D96N crystals that showed sharp reflections to high resolution (better than 3.5 Å) were analyzed.

In order to extract accurate projection intensities from the data collected from such reconstituted crystals we employed a scheme, previously developed by Mitra and Stroud (1990), for analyzing twinning, detwinning, and removal of the effects of the specimen tilt through a least-squares algorithm. For estimating the twin and tilt parameters, projection intensities and the variation of intensities as a function of reciprocal lattice coordinate z^*, near $z^* = 0$, for all lattice rods in the resolution shell 26–5 Å obtained by Henderson et al. (1990) for PM were used. The extracted projection intensities were six-fold symmetry averaged and the averaged structure factor and its variance were evaluated. All patterns were processed to 3.6-Å resolution.

The scaling between two data sets was performed using a single scale K and a temperature factor B by least squares minimizing Q where Q is given by,

$$Q = \sum_{hk} [I_1 - Ke^{-Bs_{hk}^2} I_2]^2 \quad (1)$$

where I_1 and I_2 are the symmetry averaged extracted intensities for the reflection with indices h, k, s_{hk} is the reciprocal lattice vector and the sum is over all overlapping reflections. Scaled structure factors $|F|$ were next calculated from the scaled intensity values.

The set of symmetry-averaged structure factors from each e-bR pattern was scaled to the projection data $|F(PM)|$ from PM (Henderson et al., 1990) and the structure factors were merged yielding a set of consensus e-bR structure factors $|F_N|$. The set of symmetry-averaged structure factors from each e-D96N pattern was scaled to this consensus e-bR data set and the scaled structure factors merged to yield a set of consensus e-D96N structure factors $|F_D|$. Projection maps and difference Fourier maps were synthesized using the scaled-averaged structure factors so determined, and using the phases and figures of merit determined by Henderson et al. (1990). The mean-squared error $\langle \Delta\Delta\rho^2 \rangle$ in the difference density map given as,

$$\langle \Delta\Delta\rho^2 \rangle = (1/V^2) \sum_{hk} \frac{[\Delta F^2 * (2.0 - m^2)]}{2.0} + \sigma_N^2 + \sigma_D^2, \quad (2)$$

is based on the expression given by Dickerson et al. (1961) for density maps and modified for difference maps by Henderson and Moffat (1971) and Blundell and Johnson (1976). Here σ_N and σ_D are the standard deviations calculated for $|F_N|$ and $|F_D|$, respectively. ΔF is the difference amplitude, m is the figure of merit, and the sum is over all the reflections used in the synthesis of the map. The standard deviation in the expected noise level in the difference map is given by $\Omega = (\langle \Delta\Delta\rho^2 \rangle)^{1/2}$. An absolute scale factor was calculated based on the set of PM projection amplitudes $|F(PM)|$ by assuming that the protein occupies 68% of the unit cell (Engelman et al., 1980; Hayward and Stroud, 1981) and that the average scattering density in the lipid region is 77% of that of the protein (Engelman et al., 1980). Electron scattering factors were from the International Tables for Crystallography, vol. 4.

RESULTS

A high resolution diffraction pattern at room temperature from a glucose-embedded e-D96N crystal is shown in Fig. 2. The reconstituted samples of e-bR or e-D96N consisted mainly of crystalline circular sheets and vesicles with surface lattice of trigonal P3 symmetry. Occasionally tubular vesicles with an orthorhombic surface lattice (plane group of symmetry pgg, a = 127 Å, b = 67 Å) were also present (Miercke et al., 1991). The diameter of the circular patches of reconstituted e-bR or e-D96N crystals measured 5 μm on average. In our hands (Mitra and Stroud, 1990) this is also the average size of recrystallized 2-D crystals grown from Triton X-100 solubilized PM (Cherry et al., 1978) after 2–4 weeks of dialysis to remove the detergent. Therefore the kinetics of protein reconstitution and crystal growth for e-bR and e-D96N starting from protein-lipid-detergent micelles is similar to those for w-bR.

The averaged unit cell dimension for e-bR crystals was a = 63.2 ± 0.4 Å, and for e-D96N crystals was 63.4 ± 0.3

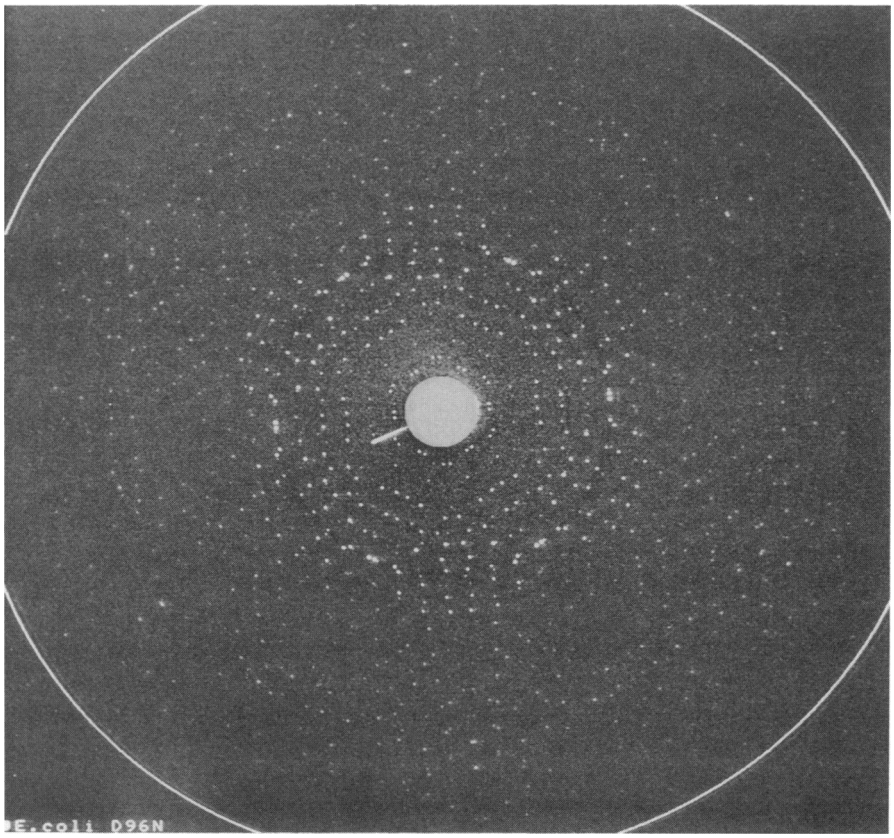

FIGURE 2 Digitized display of high resolution electron diffraction pattern from a glucose-embedded e-D96N crystal after subtracting contribution from inelastic scatter. The pattern is from two major crystalline domains inclined to each other by an angle of 8°. Diffraction spots to 2.9 Å are visible. The circular arcs represent 3.1-Å resolution.

Å. This is 62.5 Å in PM as determined by Henderson and coworkers for native membranes (Henderson and Unwin, 1975) or fused sheets (Henderson et al., 1990) at −160°C and 61.9 Å as determined by Hayward and Stroud (1981) for native membranes at −120°C. Thus there is ~1% increase in the lattice dimension in the lipid-reconstituted crystal of the *E. coli*-expressed protein. The values of R_{sym} and R_{merge} for the data from e-bR and e-D96N crystals for all reflections (26–3.6-Å resolution) and in resolution shells are presented in Table 1. In Table 2 the merged projection structure factors $|F_N|$ (for e-bR) and $|F_D|$ (for e-D96N) and their standard deviations together with the projection structure factors $|F(PM)|$ are listed.

As a function of resolution the profiles of the variations of $|F(PM)|$ and $|F_N|$, averaged in resolution shells, are compared in Fig. 3. The similarity of these profiles throughout the resolution range is apparent and the average of the difference amplitude $\langle|\Delta F|\rangle(\langle||F_N| - |F(PM)||\rangle)$ does not decrease or increase monotonically. This indicates that the wild-type crystal in PM and the reconstituted crystal of bR analog are isomorphous. Under the assumption that the 1.1% increase in unit cell dimension (62.5 to 63.2 Å) is isotropic and that no molecular reorientation has taken place in the reconstituted crystal, we estimate a 2.3% fractional change in the structure factor in the resolution range considered. This is much smaller than the observed overall fractional change $\langle||F_N| - |F(PM)||\rangle/\langle|F(PM)|\rangle$

TABLE 1 Symmetry and merging *R* factors* for the diffraction patterns from crystals of e-bR and e-D96N used in synthesizing difference Fourier maps

	e-bR, four patterns		e-D96N, five patterns	
	On I	On $\|F\|$	On I	On $\|F\|$
R_{sym}‡				
(26.0–7.0 Å)	11.5	7.3	9.1	5.8
(7.0–5.0 Å)	26.7	15.1	22.7	13.2
Overall (26.0–3.6 Å)	16.8	11.9	12.5	9.1
R_{merge}§				
(26.0–7.0 Å)	7.2	4.8	6.2	4.1
(7.0–5.0 Å)	16.8	10.0	11.8	7.8
(26.0–3.6 Å)	11.8	9.2	8.1	6.3

*Based on extracted data after correcting for twinning and tilt.

‡Average value of the agreement index. This for a given diffraction pattern calculated on the structure factors is expressed as,

$$R_{sym} = \sum_{hk}\sum_{i=1}^{n}||F_i| - \langle|F_i|\rangle| \Big/ \sum_{hk}\sum_{i=1}^{n}|F_i|$$

§Agreement index for merging of data sets calculated on the structure factors is expressed as,

$$R_{merge} = \sum_{hk}\sum_{j=1}^{N}||F_j| - |F_{merge}|| \Big/ \sum_{hk}\sum_{j=1}^{N}|F_j|$$

where $|F_j|(=\langle|F_i|\rangle)$ is the six-fold symmetry averaged value for a given reflection in a pattern and $|F_{merge}|$ is the corresponding merged value from N patterns.

TABLE 2 Averaged projection structure factors $|F|$ and their experimentally determined standard deviations σ to 3.6-Å resolution. $|F_N|$ is for merged data from e-bR crystals and $|F_D|$ is formerged data from e-D96N crystals.

H	K	$\|F(PM)\|$ *	$\|F_N\|$ ‡	σ_N‡	$\|F_D\|$ ‡	σ_D‡	H	K	$\|F(PM)\|$ *	$\|F_N\|$ ‡	σ_N‡	$\|F_D\|$ ‡	σ_D‡
1	2	10.72	9.90	0.19	9.85	0.06	6	1	13.77	13.17	0.36	13.55	0.19
1	3	5.58	5.49	0.27	5.01	0.12	6	2	5.99	5.46	0.10	5.73	0.35
1	4	13.61	14.13	0.21	12.89	0.09	6	4	5.89	3.51	0.88	5.00	0.02
1	5	15.85	15.38	0.32	15.93	0.30	6	5	2.20	4.04	1.37	3.01	0.16
1	6	4.58	3.23	0.25	4.24	0.09	6	6	1.90	2.40	0.08	1.81	0.13
1	7	13.47	12.36	0.09	12.50	0.19	6	7	6.41	4.69	0.43	5.33	0.20
1	8	4.81	4.40	0.13	4.90	0.27	6	8	9.79	8.19	0.27	9.03	0.19
1	9	3.82	3.47	0.15	3.79	0.13	6	9	2.81	2.25	0.32	2.49	0.14
1	10	3.50	4.03	0.19	3.95	0.45	6	10	3.14	3.96	0.16	2.62	0.18
1	11	3.69	4.36	0.08	3.28	0.25	6	11	1.64	2.85	0.28	1.41	0.05
1	12	10.23	8.83	0.37	9.30	0.05	7	0	10.43	9.48	0.05	9.43	0.27
1	13	8.03	8.33	0.53	7.40	0.30	7	1	9.62	8.84	0.46	9.91	0.32
1	14	2.42	2.71	0.59	4.08	0.20	7	2	2.52	2.94	0.09	3.47	0.19
2	1	5.45	6.92	0.39	5.86	0.17	7	3	5.24	5.02	0.49	4.60	0.03
2	2	13.77	13.17	0.05	13.60	0.09	7	4	1.66	2.35	0.08	1.77	0.23
2	3	8.71	7.48	0.12	7.71	0.14	7	5	3.18	3.39	0.28	2.45	0.07
2	4	22.97	22.46	0.09	22.42	0.09	7	6	4.96	4.78	0.64	3.95	0.17
2	5	6.73	7.16	0.45	7.41	0.33	7	7	7.40	7.56	0.40	7.49	0.22
2	6	7.75	7.51	0.39	8.37	0.10	7	8	1.88	2.67	0.23	1.79	0.23
2	7	10.09	8.73	0.06	9.25	0.16	7	9	3.94	4.06	0.09	3.53	0.16
2	8	8.55	8.64	0.17	8.54	0.13	8	0	3.68	3.55	0.25	3.57	0.18
2	9	8.17	6.96	0.41	7.43	0.15	8	1	0.42	2.11	0.05	1.65	0.08
2	10	6.48	6.18	0.23	6.67	0.10	8	2	6.69	6.04	0.18	6.08	0.12
2	11	6.63	5.59	0.51	6.52	0.24	8	3	5.10	5.60	0.45	5.52	0.18
2	12	5.45	5.58	0.80	4.92	0.24	8	4	2.63	3.58	0.32	3.14	0.17
2	13	2.06	2.18	2.18	2.47	0.21	8	5	7.70	7.59	0.30	7.96	0.12
2	14	1.20	1.92	0.09	1.54	0.20	8	6	5.94	4.26	0.78	3.96	0.27
3	0	6.70	5.44	0.20	4.78	0.12	8	7	5.57	4.61	0.21	4.03	0.14
3	1	16.86	15.12	0.29	16.13	0.12	8	8	6.00	5.45	0.45	4.43	0.16
3	2	13.16	12.32	0.49	13.75	0.33	8	9	4.29	4.85	0.10	5.27	0.02
3	3	1.64	3.60	0.27	4.16	0.28	9	0	4.40	4.32	0.14	3.94	0.28
3	4	15.53	17.17	0.32	17.79	0.31	9	1	9.29	7.94	0.21	7.57	0.08
3	5	15.32	16.86	0.51	15.86	0.14	9	2	4.81	4.78	0.40	5.00	0.10
3	7	6.34	6.84	0.19	7.18	0.26	9	3	6.53	5.98	0.20	6.61	0.08
3	8	4.46	4.04	0.44	4.26	0.13	9	4	4.14	2.69	0.15	3.44	0.19
3	9	1.81	2.33	0.20	2.49	0.13	9	5	7.34	5.98	0.13	5.79	0.26
3	10	2.35	2.72	0.13	2.61	0.03	9	6	4.86	3.41	0.44	3.88	0.09
3	11	7.14	5.96	0.56	6.68	0.17	9	7	1.97	2.64	0.62	1.41	0.11
3	12	4.73	5.14	0.31	4.42	0.19	9	8	2.82	3.44	0.19	3.76	0.23
3	13	2.86	2.86	0.31	2.27	0.13	10	0	4.43	3.62	0.25	3.03	0.15
4	0	13.59	12.26	0.34	12.59	0.06	10	1	2.50	3.54	0.27	2.89	0.20
4	1	17.07	15.94	0.17	15.56	0.28	10	2	6.67	5.51	0.28	5.94	0.17
4	2	10.16	9.59	0.49	9.33	0.03	10	3	8.89	7.66	0.25	7.60	0.14
4	3	25.24	26.93	0.42	26.25	0.41	10	4	2.12	2.66	0.32	2.04	0.09
4	4	6.64	6.71	0.51	6.63	0.27	10	5	6.57	5.83	0.39	5.73	0.21
4	5	5.53	5.87	0.80	6.28	0.18	10	6	2.71	3.12	0.36	2.16	0.02
4	6	4.07	4.62	0.67	3.04	0.49	11	0	5.42	5.07	0.16	5.17	0.35
4	7	4.78	5.23	0.35	4.88	0.03	11	1	4.70	2.92	0.22	4.05	0.32
4	8	3.57	3.79	0.36	3.99	0.25	11	2	5.87	3.81	0.51	4.33	0.12
4	9	4.93	5.04	0.64	5.96	0.14	11	3	5.63	5.57	0.17	5.79	0.09
4	10	6.82	5.93	0.18	5.98	0.10	11	4	1.35	2.58	0.12	1.51	0.14
4	11	2.62	3.77	0.62	3.36	0.18	11	5	4.65	6.23	0.33	4.32	0.20
4	12	3.09	4.04	0.57	2.59	0.16	11	6	1.57	2.82	0.45	1.75	0.22
5	0	20.71	19.14	0.18	19.26	0.19	12	0	5.45	5.20	0.33	6.01	0.17
5	1	5.63	5.55	0.50	4.78	0.45	12	1	2.18	2.37	0.09	3.16	0.48
5	2	17.47	17.83	0.25	17.88	0.28	12	2	2.03	2.54	0.12	2.03	0.14
5	3	5.55	4.06	1.12	4.17	0.19	12	3	1.76	2.83	0.21	2.25	0.23
5	4	2.95	2.17	2.17	3.12	0.11	12	4	2.05	2.18	0.26	2.07	0.13
5	5	3.78	3.15	0.27	2.78	0.05	13	0	3.90	3.10	0.16	3.40	0.02
5	6	3.77	3.14	1.24	3.12	0.05	13	1	5.23	4.38	0.74	5.26	0.25
5	7	6.53	3.82	0.41	4.59	0.17	13	2	6.49	5.70	0.84	5.36	0.25
5	8	3.12	2.26	0.22	2.26	0.10	13	3	1.99	3.25	0.09	2.68	0.16
5	9	1.61	2.42	0.29	1.80	0.12	14	0	3.01	2.72	0.20	3.28	0.37
5	10	2.18	2.32	0.20	1.87	0.12	14	1	5.90	5.97	0.24	4.94	0.20
5	11	3.25	2.62	0.26	2.95	0.14	14	2	3.18	3.38	0.26	3.10	0.16
6	0	12.68	11.94	0.36	12.22	0.20	15	0	6.03	5.07	2.46	5.49	0.16

* Projection structure factors for PM from Henderson et al. (1990).

‡ Each $|F_N|$ and $|F_D|$ are obtained through merge of, on average, 21.5 and 26.5 separate observations, respectively, for the same reflection and are given as,

$$F = \sum_{j=1}^{N} \frac{F_j}{\sigma_j^2} \Bigg/ \sum_{j=1}^{N} \frac{1.0}{\sigma_j^2}$$

where σ_j is the standard deviation in the extracted sixfold averaged structure factor F_j for the jth pattern and N is the number of patterns averaged. The overall standard deviation σ for the merged $|F|$ values are given as

$$\sigma = \left[\sum_{j=1}^{N} \frac{(F_j - F)^2}{\sigma_j^2} \Bigg/ N \sum_{j=1}^{N} \frac{1.0}{\sigma_j^2} \right]^{1/2}.$$

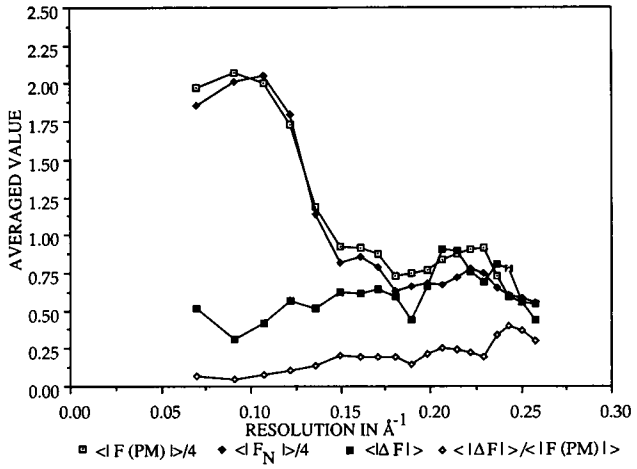

FIGURE 3 Resolution dependence of scaled and merged projection structure factors ($|F_N|$) for e-bR crystal compared to those for PM (Henderson et al., 1990). Each point of the graph is for a bin of 12 reflections centered at that resolution. $|\Delta F| = ||F_N| - |F(PM)||$.

of 12.7%. The projection density map at 3.6-Å resolution for e-bR is shown in Fig. 4 *a*. The difference Fourier map synthesized with the amplitudes $|F_N| - |F(PM)|$ is shown in Fig. 4 *b*. This map describes, relative to w-bR, the sites and the magnitudes of the observed changes in projection in the structure of e-bR. Fig. 4 *c* is a difference map calculated between two independent subsets each comprising of two merged e-bR data sets. This map describes the contribution of the errors in the amplitudes within the e-bR data sets to features in the difference map shown in Fig. 4 *b*. The relative strengths of the peaks and valleys in Fig. 4 *b* can be estimated from the calculated integrated density of the broad peak marked I in the lipid region which, based on an absolute scaling, represents change equivalent to approximately 7 carbon atoms.

In Fig. 5, as a function of resolution, the profiles of the variations of $|F_D|$ and $|F_N|$, averaged in resolution shells, are compared. The e-D96N crystal is isomorphous to e-bR crystal to the highest resolution we have studied. The observed fractional change in averaged structure factors between e-D96N and e-bR given by $\langle||F_D)| - |F_N||\rangle/\langle|F_N|\rangle$ ranges from 4.8% at low resolution (26–7 Å) to 13.0% at high resolution (7–3.6 Å) with an overall value of 9.2%. These changes are smaller than what we observe between data from e-bR and PM.

We estimated how much of the observed fractional change between e-bR and e-D96N data corresponds to signal in two ways as follows.

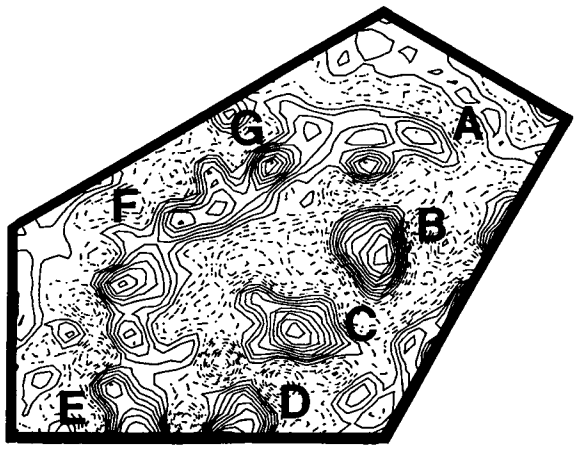

a

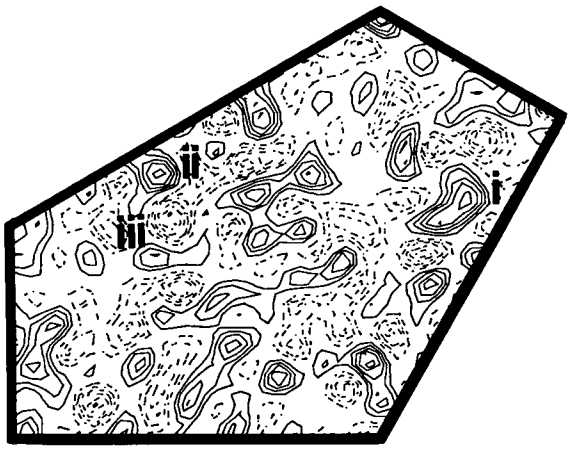

b

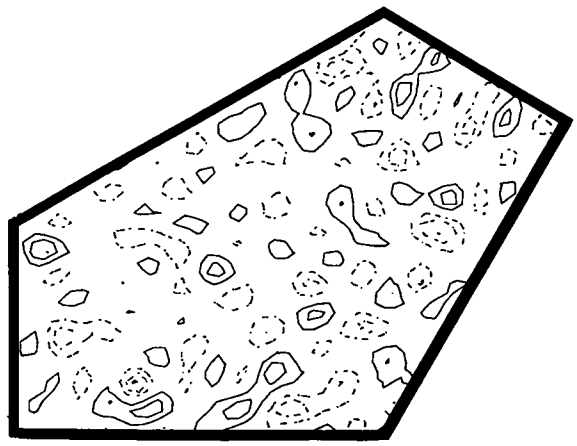

c

FIGURE 4 (*a*) Projection density map of e-bR at 3.6-Å resolution calculated using amplitudes $|F_N|$ (Table 2), and using phases determined by Henderson et al. (1990). The contour interval is 4.73 times that used in Fig. 6 *a*. (*b*) Projection Fourier difference map calculated to 3.6-Å resolution using the difference amplitudes $|F_N| - |F(PM)|$. (*c*) Projection Fourier difference map calculated between two independent subsets of merged e-bR data sets. Solid lines represent positive and dashed lines negative contour levels. The contour interval is the same as in Fig. 6 *a*.

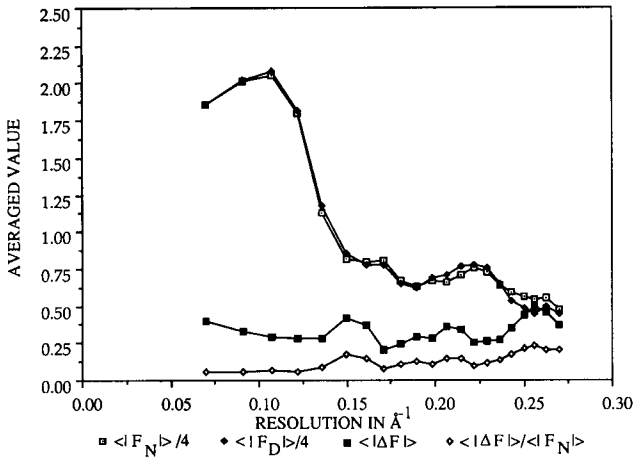

FIGURE 5 Resolution dependence of scaled averaged projection structure factors for e-bR and e-D96N crystals. Each point of the graph is for a bin of 12 reflections centered at that resolution. $|\Delta F| = ||F_D| - |F_N||$.

1) From the four scaled e-bR data sets, all six possible e-bR subsets, each produced by a merger of various combinations of two e-bR data sets were created. Similarly from the five e-D96N data sets all 10 possible e-D96N subsets, each produced by a merger of various combinations of two (or three) e-D96N data sets were created. From these subsets, all 60 possible sets of pairs of difference intensities $(\Delta I)_1$ and $(\Delta I)_2$ that did not contain data from any common e-bR or e-D96N data set were calculated. Next sample correlation coefficients (r) between all these 60 pairs of independent sets of difference amplitudes and the estimated "true" change (Glaeser et al., 1986) $\langle|\Delta I|\rangle_s$ in each case given by

$$\langle|\Delta I|\rangle_s = r * \sqrt{\langle|\Delta I|\rangle_1 * \langle|\Delta I|\rangle_2} \tag{3}$$

were determined. The calculated averaged value $\langle r\rangle$ was 0.20 and in comparison $\langle r\rangle$ was 0.02 when the difference intensities calculated within the e-bR subsets were correlated with those calculated within the e-D96N subsets. Using Student's t test, for an average comparison of 120 pairs of $|\Delta I|$ a value of $r = 0.20$ is at better than 98% level of significance. From the average of 60 values of $\langle|\Delta I|\rangle_s$, the estimated "noise-free" contribution to fractional intensity change is calculated to be 5.5%. Using the expression

$$N_m = N * (\langle|\Delta I|\rangle_s/\langle I\rangle)^2 \tag{4}$$

from Crick and Magdoff (1956) to quantitate the number of atoms N_m moved in a structure composed of N atoms corresponding to a given fractional change in intensity, we find that for 2300 nonhydrogen atoms in PM a 5.5% change translates to movement involving about 7 nonhydrogen atoms.

2) Assuming that the merged intensity I with standard deviation σ_I $(= 2.0 * |F| * \sigma)$ follows a normal distribution, the difference intensity $\Delta I = I_D - I_N$ is normally distributed with a standard deviation $\sigma'_I = \sqrt{\sigma^2_{NI} + \sigma^2_{DI}}$. Histogram plots of scaled extracted intensity values of symmetry mates for example reflections (4, 3), (3, 4), (11, 3), and (3, 11) from five e-D96N patterns showed that a normal distribution is a good approximation (average coefficient of correlation with a normal distribution was 0.80 which is at better than 95% significance level from Student's t test (Weatherburn, 1961)). A smoothed profile for the variation of σ'_I as a function of resolution was obtained by weighted least-squares fitting a fourth order polynomial to the averaged values of σ'_I calculated in resolution shells. The noise estimate $E|\Delta I|$ in $|\Delta I|$ for a given reflection is given as the mean deviation from the mean value of ΔI (the observed difference intensity). This, for a normal distribution for ΔI is equal to $\sigma'_I * \sqrt{2/\pi}$ (Weatherburn, 1961) where for a given reflection, the value of σ'_I obtained from the fitted polynomial is used. The observed averaged fractional change in intensities, the estimated contribution to this change from noise calculated as above, and the "signal" defined as the difference of the two are listed in Table 3 for various resolution shells.

Fig. 6 *a* shows the difference Fourier map at 3.6-Å resolution calculated with amplitudes $\Delta F = |F_D| - |F_N|$ and the same overlaid on an outline of the projection density map of e-bR (Fig. 6 *b*). In order to quantitate the contribution of noise in the e-bR and e-D96N data sets to that in the difference map in Fig. 6 *a* we synthesized a map at 3.6-Å resolution (Fig. 7) using as amplitudes $\pm E|\Delta F|$ where $E|\Delta F|$ is the estimated error in the difference amplitude $|\Delta F|$ and the signs were generated randomly. The estimated error $E|\Delta F|$ is calculated from $E|\Delta I|$ as follows. We have,

$$\begin{aligned} |\Delta F| &= ||F_D| - |F_N|| \\ &= |\Delta I|/(||F_D| + |F_N||) \\ &\approx |\Delta I|/[2.0 * (I_N)^{1/2}] \end{aligned} \tag{5}$$

By taking the derivative of both sides we can then write $E|\Delta F|$ as,

$$E|\Delta F| \approx \frac{E|\Delta I|}{2.0 * (I_N)^{1/2}} + \frac{|\Delta I| * E(I_N)}{4.0 * (I_N)^{3/2}} \tag{6}$$

Here $E(I_N)$ is the estimated error in I_N and is calculated by the same method as was employed for obtaining $E|\Delta I|$ described above.

TABLE 3 Observed (ϕ) averaged fractional changes in intensities between data from e-D96N and e-bR, estimated contribution of noise (ν) to this change and the estimated true fractional change (ψ).

Resolution	ϕ	ν	ψ
	%	%	%
(26.0–7.0 Å)	7.2	3.8	3.4
(7.0–5.0 Å)	17.4	14.2	3.2
(5.0–3.6 Å)	23.5	13.7	9.8
Overall (26.0–3.6 Å)	11.3	6.7	4.6

$\phi = \langle|\Delta I|\rangle/\langle I\rangle$, $\nu = \langle E|\Delta I|\rangle/\langle I\rangle$, where $E|\Delta I|$ is the estimated noise in the difference intensity $\Delta I = (|F_D|^2 - |F_N|^2)$ (see section on Results). $\psi = \phi - \nu$. $I = |F|^2$.

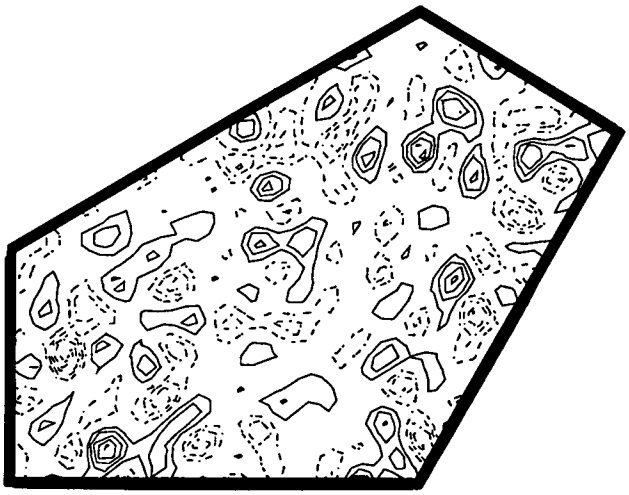

a

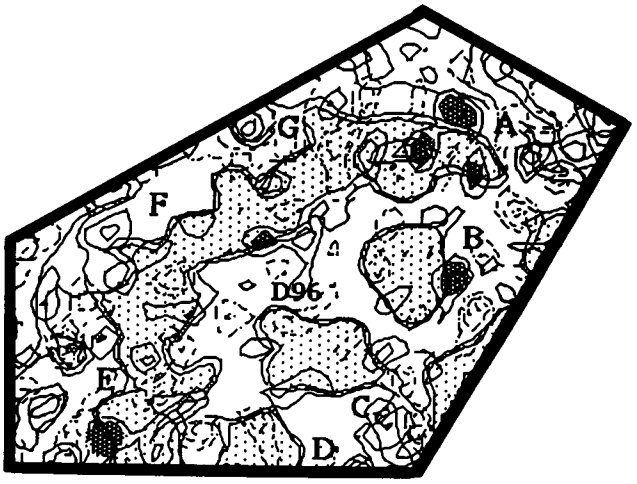

b

FIGURE 6 (*a*) Projection Fourier difference map calculated to 3.6-Å resolution using the difference amplitudes $|F_D| - |F_N|$. Solid lines represent positive and dashed lines negative contour levels. The contour interval is one standard deviation Ω of the expected noise level (Eq. 2). (*b*) The difference map in *a* with the significant peaks shaded dark is overlaid on the e-bR projection map. The locations in projection of the bR helices A (amino-terminal) to G (carboxyl-terminal) and the position of Asp^{96} as in the three-dimensional model of bR (Henderson et al., 1990) are indicated.

In the map shown in Fig. 6 *a*, the integrated scattering potentials of all peaks or valleys within and in the neighborhood of the protein envelope are $<\sim 3$ carbon atoms being about 0.7% of average scattering potential of one transmembrane bR helix.

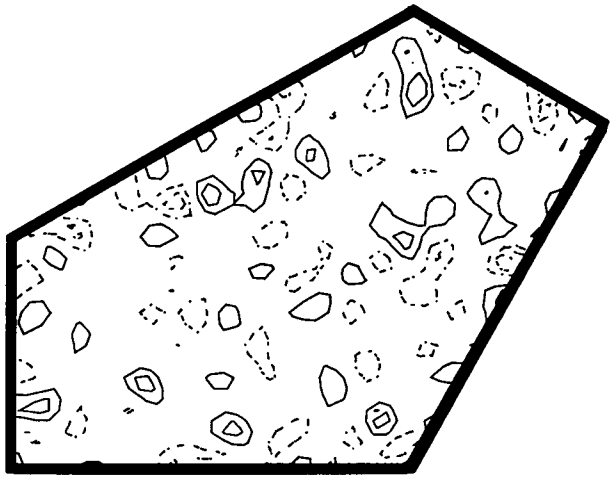

FIGURE 7 A "noise" map at 3.6-Å resolution synthesized with amplitudes as the expected errors in the difference amplitudes $|F_D| - |F_N|$ (see section on Results for the method of calculating expected errors). The contour interval is the same as in Fig. 6 *a*.

DISCUSSION

The functional importance of one or more substituted residues in a functionally altered variant of a protein remains unresolved until high resolution structural studies are carried out to determine structural perturbations, if any, due to alteration/s in the amino acid sequence. This study, representing the first high resolution structural analyses of the effects of a single-site mutation in an expressed membrane protein addresses this question for the D96N variant of bR.

e-bR

The difference Fourier map in Fig. 4 *b* synthesized with the amplitudes $|F_N| - |F(PM)|$ shows a number of peaks and valleys distributed within the protein envelope and in its neighborhood. In comparison the companion "noise" map (Fig. 4 *c*) is relatively featureless. The features in the difference map in Fig. 4 *b* arise from protein conformational change in e-bR and/or rearrangements of the lipids in the lipid-reconstituted e-bR crystal relative to PM. Since the structure factors for PM (Henderson et al., 1990) were measured at −160°C and those for e-bR crystal (this work) are measured at room temperature, some of these changes could be due to temperature-induced structural perturbations in the bR-lipid crystal. In the protein envelope the largest of the peaks and valleys are at helices F, G, and at helix C. At helix F, for instance, the integrated densities and their 4-Å separation for the peak(II)/valley(III) pair, represent a calculated moment of ~30 eÅ. This could represent an outward (toward surrounding lipids) movement of ~5 C-atom equivalents through ~3 Å or to an outward movement of <0.1 Å of helix F. The broad peak marked *I* near the amino-terminal helix A was reproducibly seen in both the e-bR-PM difference map (shown) as well as in e-D96N-PM difference map (not shown), and could represent the density corresponding to

extra amino-terminal residues in the fusion protein. The integrated potential of 7 C-atoms in this peak corresponds to only about 1.5 amino acids, far less than the expected ~10 amino acids based on the estimated proportions of the amino-terminal-processed bR polypeptides in PM (Miercke et al., 1989) and in e-bR (Shand et al., 1991). Even considering that any signal in a difference-Fourier map is expected to appear at half its actual size, this peak would correspond at best to three amino acids or to about 30% occupancy of the extra amino terminus amino acids in the fusion protein. This would suggest that the elongated amino terminus in this bR analog is quite disordered as in PM (Henderson et al., 1990).

e-D96N

It is known that azide, sometimes used as an antimicrobial agent in buffer solutions, can functionally replace D96 in D96N as a surrogate proton donor and acceptor (Tittor et al., 1989) to reversibly restore wild-type activity. To separate any possible electronic and/or induced structural effect of azide on the mutant protein structure, we removed azide from crystallized e-D96N prior to sample preparation for electron diffraction by washing with large excess of azide-free buffer.

Table 3 shows that the estimated "true" averaged fractional change in intensities between e-D96N and e-bR data defined as the difference of the observed and the estimated contribution of noise is largest (9.8%) at high resolution (5–3.6 Å) with small contributions (~3.3%) at low resolution. This means that relative to e-bR changes in e-D96N primarily involve movements of atoms through distances that are likely to be ~4 Å or less. The "noise" map shown in Fig. 7 synthesized with the estimated errors in the e-D96N-e-bR difference amplitudes describes the sizes of peaks and valleys that are expected from the contribution of random noise alone in the consensus difference map shown in Fig. 6 *a*. The minimum and maximum values of density in the "noise" map was found to be very close to -3Ω and 3Ω, respectively (Ω is the estimated standard deviation in the noise level of the difference map in Fig. 6 *a* calculated using Eq. 2) which is equal to the threshold at which a peak or a valley is considered statistically reliable in a map.

The magnitudes of the changes between e-D96N and e-bR given as the integrated densities of the peaks and valleys in the difference map (Fig. 6 *a*) are small being <~3 C-atom equivalents. At the site of substitution itself in helix C, as seen from Fig. 6 *a*, there are no 3Ω level peaks or valleys indicating that there are no significant structural change in this helix. In Fig. 6 *a*, within the protein envelope, five of the six largest peaks and valleys, at helices A, B, and between F and G are at the 3Ω level (integrated density, ~2 C-atoms) and the other at helix E is at the 4Ω level (integrated density ~3 C-atoms). The peak between helices F and G, closest to the site of substitution, is at a projected distance of 6.5 Å from this site. The strongest peak at 4Ω level is at helix E, ~20 Å away in projection from the site of substitution. There is a valley ~6 Å away from this peak toward the interior of the protein and the integrated densities and separation of this peak/valley pair (moment ~ 40 eÅ) correspond to movements of ~5 C-atom equivalents through ~4 Å or to an inwards shift of helix E by <0.1 Å. The other peak and valley pair at helix B could represent smaller outward (toward surrounding lipids) movements in the form of ~2 C-atoms through ~3 Å.

Recent x-ray diffraction studies (Dencher et al., 1991; Koch et al., 1991) on D96N mutant derived from *Halobacterium* sp. GRB (Soppa and Oesterhelt, 1989) have investigated structural changes at pH 9.6 in going from bR to the M_{412} state by exploiting the presence of a long-lived M_{412} intermediate in this mutant. In order that such observed structural changes in the photo-intermediate may faithfully reproduce those occurring in the wild-type protein, it is implicitly assumed in such investigations that the ground-state structures of wild-type bR and D96N are very similar. As shown in the difference map in Fig. 6 *a* this assumption is essentially correct particularly within the vicinity (5 Å projected distance) of the site of substitution.

Asp^{96} is protonated in the ground state up to pH 10 (Engelhard et al., 1990; Metz et al., 1992). Thus its replacement by neutral Asn does not constitute any charge imbalance within the interior of the protein. In the latter half of the photocycle, however, during the M → N transition, Asp^{96} is deprotonated (Bousche et al., 1991) which probably produces local electrostatic and/or conformational perturbations due either to increased solvent accessibility of the now negatively charged side chain or to formation of a salt bridge with a positively charged side chain in the protein. In D96N such a deprotonation is chemically hindered, and the photocycle proceeds through diffusion-controlled reprotonation of the Schiff base from the bulk medium. Thus it is possible that relative to the wild type there are stronger structural fluctuations in the D96N mutant in the latter half of the photocycle (Thorgeirsson et al., 1991).

After submission of this manuscript Subramaniam et al. (1993) using membranes isolated from strains of *H. halobium* (sp. GRB) carrying the D96G mutation published analysis of structural changes between bR ground state and the M state with samples preserved in vitreous ice. These authors concluded that the ground-state structures of D96G and PM are very similar. This was based on a D96G – PM difference Fourier map (Fig. 3 *b* in their article) that was however an average of maps obtained in vitreous ice and those obtained from glucose-embedded samples. It should be noted that Jaffe and Glaeser (1987) have observed from difference maps calculated at 4.25-Å resolution that there are structural variations in PM between glucose embedded and vitreous ice environments. It is possible that between these two environments in the vicinity of Asp^{96} or elsewhere there are structural differences the signals from which could fortuitously diminish or cancel out in an averaged difference map. Thus even though our conclusion is similar in relation to the lack of structural change in the ground state of mutant Asp^{96} with respect to the wild type, our data proves the point more clearly.

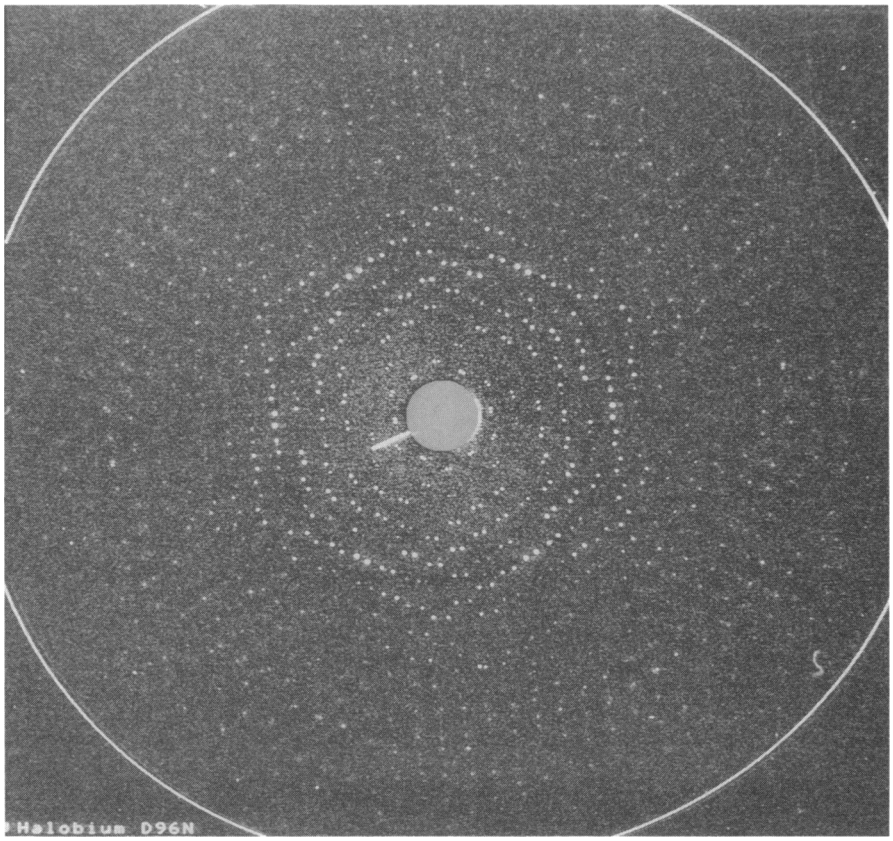

FIGURE 8 Digitized display of high resolution electron diffraction pattern from glucose embedded h-D96N crystal after subtracting contribution from inelastic scatter. The two major overlapping lattices are inclined to each other by an angle of 4°. Diffraction spots to 2.9 Å are visible. The circular arcs represent 3.1-Å resolution.

We have in this work established a formalism for investigating induced structural changes at high resolution at the level of 2–3 carbon atom equivalents in bacteriorhodopsin variants. With the advent of a DNA transformation system for *Halobacterium* (Cline et al., 1989) such investigations on *H. Halobium*-expressed bR variants that form highly ordered crystalline arrays in vivo (Fig. 8) are possible for the ground state and in trapped intermediates.

CONCLUSION

1) We have developed a protocol that generates large (~5-μm average diameter) 2-D crystals of *E. coli*-expressed bacteriorhodopsin and its variant D96N starting with opsin protein purified in SDS. These crystals diffract to better than 3.0-Å resolution at room temperature and have a lattice homologous to the P3 lattice in PM or in transformed PM. This is the first instance of an integral membrane protein yielding 2-D crystals of such high order after being purified from the denaturing detergent SDS.

2) The structural alterations determined in *E. coli*-expressed variants should faithfully reproduce the situation in the PM. The Fourier difference map at 3.6-Å resolution (Fig. 4 *b*) shows that the structure of e-bR is similar to that of w-bR in PM with no global structural rearrangements. This agrees with our previous similar conclusions from observations that e-bR has a rate of retinal incorporation, dark and light-adapted absorption properties, light-induced proton pumping activity (Miercke et al., 1991), photocycle kinetics (Milder et al., 1991), and chromophore geometry and environment (Lin et al., 1991) identical to those for w-bR.

3) The difference map (Fig. 6 *a*) shows that for the isosteric substitution of Asp^{96} by Asn, the molecular conformation in the fusion bR analog in the ground state is essentially unaltered. This, therefore, proves that the known effect of this mutation in terms of slowing down the decay of the M_{412} intermediate (Holz et al., 1989) is not due to ground-state structural perturbations and that the carboxylate moiety is indeed critical for the proton translocation.

This work was supported by the National Institutes of Health grants GM32079 (to R. M. Stroud) and GM31785 (to M. C. Betlach).

REFERENCES

Blaseio, U., and F. Pfeifer. 1990. Transformation of *Halobacterium halobium*: development of vectors and investigation of gas vesicle synthesis. *Proc. Natl. Acad. Sci. USA.* 87:6772–6776.

Blundell, T. L., and L. N. Johnson. 1976. *In* Protein Crystallography. Academic Press, London. 409–411.

Bousche, O., M. S. Braiman, Y. W. He, T. Marti, H. G. Khorana, and K. J. Rothschild. 1991. Vibrational spectroscopy of bacteriorhodopsin mutants. Evidence that Asp-96 deprotonates during the M → N transition. *J. Biol. Chem.* 266:11063–11067.

Braiman, M. S., T. Mogi, T. Marti, L. J. Stern, H. G. Khorana, and K. J. Rothschild. 1988. Vibrational spectroscopy of bacteriorhodopsin mutants: light-driven proton transport involves protonation changes of aspartic acid residues 85, 96, and 212. *Biochemistry.* 27:8516–8520.

Cherry, R. J., U. Muller, R. Henderson, and M. P. Heyn. 1978. Temperature-dependent aggregation of bacteriorhodopsin in dipalmitoyl- and dimyristoylphosphatidylcholine vesicles. *J. Mol. Biol.* 121:283–298.

Cline, S. W., L. C. Schalkwyk, and F. Doolittle. 1989. Transformation of the archaebacterium *Halobacterium volcanii* with genomic DNA. *J. Bacteriol.* 171:4887–4891.

Crick, F. H. C., and B. S. Magdoff. 1956. The theory of the method of isomorphous replacement for protein crystals. *Acta Crystallogr.* 9:901–908.

Dencher, N. A., J. Heberle, C. Bark, M. H. J. Koch, G. Rapp, D. Oesterhelt, K. Bartels, and G. Buldt. 1991. Proton translocation and conformational changes during the bacteriorhodopsin photocycle–time-resolved studies with membrane-bound optical probes and x-ray diffraction. *Photochem. Photobiol.* 54:881–887.

Dickerson, R. E., J. C. Kendrew, and B. E. Strandberg. 1961. The crystal structure of myoglobin: phase determination to resolution of 2 Å by the method of isomorphous replacement. *Acta Crystallogr.* 14:1188–1195.

Engelhard, M., B. Hess, G. Metz, W. Kreutz, F. Siebert, J. Soppa, and D. Oesterhelt. 1990. High resolution ^{13}C-solid state NMR of bacteriorhodopsin: assignment of specific aspartic acids and structural implications of single site mutations. *Eur. Biophys. J.* 18:17–24.

Engelman, D. M., R. Henderson, A. D. McLachlan, and B. A. Wallace. 1980. Path of polypeptide in bacteriorhodopsin. *Proc. Natl. Acad. Sci. USA.* 77:2023–2027.

Gerwert, K., B. Hess, J. Soppa, and D. Oesterhelt. 1989. Role of aspartate-96 in proton translocation by bacteriorhodopsin. *Proc. Natl. Acad. Sci. USA.* 86:4943–4947.

Glaeser, R. M., J. Baldwin, T. A. Ceska, and R. Henderson. 1986. Electron diffraction analysis of the M_{412} intermediate of bacteriorhodopsin. *Biophys. J.* 50:913–920.

Grzesiek, S., and N. A. Dencher. 1986. Time-course and stoichiometry of light-induced proton release and uptake during the photocycle of bacteriorhodopsin. *Fed. Eur. Biochem. Soc.* 208:337–342.

Hayward, S. H., and R. M. Stroud. 1981. Projected structure of purple membrane determined to 3.7 Å resolution by low temperature electron microscopy. *J. Mol. Biol.* 151:491–517.

Henderson, R., and J. K. Moffat. 1971. The difference Fourier technique in protein crystallography: errors and their treatment. *Acta Crystallogr.* B27: 141–1420.

Henderson, R., and P. N. T. Unwin. 1975. Three-dimensional structure of purple membrane obtained by electron microscopy. *Nature (Lond.).* 275: 28–32.

Henderson, R., J. M. Baldwin, T. A. Ceska, F. Zemlin, E. Beckmann, and K. H. Downing. 1990. Model for the structure of bacteriorhodopsin based on high-resolution electron cryo-microscopy. *J. Mol. Biol.* 213: 899–929.

Holz, M., L. A. Drachev, T. Mogi, H. Otto, A. D. Kaulen, M. P. Heyn, V. P. Skulachev, and H. G. Khorana. 1989. Replacement of aspartic acid-96 by asparagine in bacteriorhodopsin slows both the decay of the M intermediate and the associated proton movement. *Proc. Natl. Acad. Sci. USA.* 86:2167–2171.

Jaffe, J. S., and R. M. Glaeser. 1987. Difference Fourier analysis of "surface features" of bacteriorhodopsin using glucose-embedded and frozen-hydrated purple membrane. *Ultramicroscopy.* 23:17–28.

Karnik, S. S., M. Nassal, T. Doi, E. Jay, V. Sgaramella, and H. G. Khorana. 1987. Structure-function studies on bacteriorhodopsin. II. Improved expression of the bacterio-opsin gene in *Escherichia coli. J. Biol. Chem.* 262:9255–9267.

Kates, M., S. C. Kushwaha, and G. D. Sprott. 1982. Lipids of purple membrane from extreme halophiles and methanogenic bacteria. *Methods Enzymol.* 88:98–111.

Katre, N. V., J. F. Moore, S. Hayward, and R. M. Stroud. 1984. Location of an extrinsic label in the primary and tertiary structure of bacteriorhodopsin. *Biophys. J.* 46:195–203.

Khorana, H. G. 1988. Bacteriorhodopsin, a membrane protein that uses light to translocate protons. *J. Biol. Chem.* 263:7439–7442.

Koch, M. H., N. A. Dencher, D. Oesterhelt, H. J. Plohn, G. Rapp, and G. Buldt. 1991. Time-resolved X-ray diffraction study of structural changes associated with the photocycle of bacteriorhodopsin. *EMBO J.* 10:521–526.

Lanyi, J. K. 1992. Proton transfer and energy coupling in the bacteriorhodopsin photocycle. *J. Bioenerg. Biomembr.* 24:169–179.

Lin, S. W., S. P. Fodor, L. J. W. Miercke, M. C. Betlach, R. M Stroud, and R. A. Mathies. 1991. Resonance Raman spectra of bacteriorhodopsin mutants with substitutions at Asp-85, Asp-96, and Arg-92. *Photochem. Photobiol.* 53:341–346.

Lozier, R. H., R. A. Bogomolni, and W. Stoeckenius. 1975. Bacteriorhodopsin, a light-driven proton pump in *Halobacterium halobium. Biophys. J.* 15:955–962.

Lozier, R. H., A. Xie, J. Hofrichter, and G. M. Clore. 1992. Reversible steps in the bacteriorhodopsin photocycle. *Proc. Natl. Acad. Sci. USA.* 89:3610–3614.

Mathies, R. A., C. H. Brito Cruz, W. T. Pollard, and C. V. Shank. 1988. Direct observation of the femtosecond excited-state *cis-trans* isomerization in bacteriorhodopsin. *Science (Wash. DC).* 240:777–779.

Mathies, R. A., S. W. Lin, J. B. Ames, and W. T. Pollard. 1991. From femtoseconds to biology: mechanism of bacteriorhodopsin's light-driven proton pump. *Annu. Rev. Biophys. Biophys. Chem.* 20:491–518.

Metz, G., F. Siebert, and M. Engelhard. 1992. High-resolution solid state ^{13}C NMR of bacteriorhodopsin: characterization of [4-^{13}C]Asp resonances. *Biochemistry.* 31:455–462.

Miercke, L. J. W., P. E. Ross, R. M. Stroud, and E. A. Dratz. 1989. Purification of bacteriorhodopsin of mature and partially processed forms. *J. Biol. Chem.* 264:7531–7535.

Miercke, L. J. W., M. C. Betlach, A. K. Mitra, R. F. Shand, S. K. Fong, and R. M. Stroud. 1991. Wild-type and mutant bacteriorhodopsins D85N, D96N, and R82Q: purification to homogeneity, pH dependence of pumping, and electron diffraction. *Biochemistry.* 30:3088–3098.

Milder, S. J., T. E. Thorgeirsson, L. J. W. Miercke, R. M. Stroud, and D. S. Kliger. 1991. Effects of detergent environments on the photocycle of purified monomeric bacteriorhodopsin. *Biochemistry.* 30:1751–1761.

Mitra, A. K., and R. M. Stroud. 1990. High sensitivity electron diffraction analysis. A study of divalent cation binding to purple membrane. *Biophys. J.* 57:301–311.

Needleman, R., M. Chang, B. Ni, G. Varo, J. Fornes, S. H. White, and J. K. Lanyi. 1991. Properties of Asp212 → Asn bacteriorhodopsin suggest that Asp212 and Asp85 both participate in a counterion and proton acceptor complex near the Schiff base. *J. Biol. Chem.* 266: 11478–11484.

Oesterhelt, D., J. Tittor, and E. Bamberg. 1992. A unifying concept for ion translocation by retinal proteins. *J. Bioenerg. Biomembr.* 24:181–191.

Otto, H., T. Marti, M. Holz., T. Mogi, M. Lindau, H. G. Khorana, and M. P. Heyn. 1989. Aspartic acid-96 is the internal proton donor in the reprotonation of the Schiff base of bacteriorhodopsin. *Proc. Natl. Acad. Sci. USA.* 86:9228–9232.

Rothschild, K. J. 1992. FTIR difference spectroscopy of bacteriorhodopsin: toward a molecular model. *J. Bioenerg. Biomembr.* 24:147–167.

Rothschild, K. J., M. Zagaeske, and W. A. Cantore. 1981. Conformational changes of bacteriorhodopsin detected by Fourier transform infrared difference spectroscopy. *Biochem. Biophys. Res. Commun.* 103: 483–489.

Shand, R. F., L. J. W. Miercke, A. K. Mitra, S. K. Fong, R. M. Stroud, and M. C. Betlach. 1991. Wild-type and mutant bacterioopsins D85N, D96N, and R82Q: high-level expression in *Escherichia coli. Biochemistry.* 30: 3082–3088.

Soppa, J., and D. Oesterhelt. 1989. Bacteriorhodopsin mutants of *Halobacterium* sp. GRB. I. The 5-bromo-2′-deoxyuridine selection as a method to isolate point mutants in *Halobacteria. J. Biol. Chem.* 264:13043–13048.

Stoeckenius, W., and R. A. Bogomolni. 1982. Bacteriorhodopsin and related pigments of halobacteria. *Annu. Rev. Biochem.* 51:587–616.

Subramaniam, S., M. Gerstein, D. Oesterhelt, and R. Henderson. 1993. Electron diffraction analysis of structural changes in the photocycle of bacteriorhodopsin. *EMBO (Eur. Mol. Biol. Organ) J.* 12:1–8.

Thorgeirsson, T. E., S. J. Milder, L. J. W. Miercke, M. C. Betlach, R. F.

Shand, R. M. Stroud, and D. S. Kliger. 1991. Effects of Asp-96—-Asn, Asp-85 → Asn, and Arg-82 → Gln single-site substitutions on the photocycle of bacteriorhodopsin. *Biochemistry.* 30:9133–9142.

Tittor, J., C. Soell, D. Oesterhelt, H. J. Butt, and E. Bamberg. 1989. A defective proton pump, point-mutated bacteriorhodopsin Asp^{96} → Asn is fully reactivated by azide. *EMBO (Eur. Mol. Biol. Organ) J.* 8:3477–3482.

Trissl, H.-W. 1990. Photoelectric measurements of purple membranes. *Photochem. Photobiol.* 51:793–818.

Turner, G. J., L. J. W. Miercke, T. E. Thorgeirsson, D. S. Kliger, M. C. Betlach, and R. M. Stroud. 1993. Bacteriorhodopsin D85N–3 spectroscopic species in equilibrium. *Biochemistry.* 32:1332–1337.

Wagner, G., D. Oesterhelt, G. Krippahl, and J. K. Lanyi. 1983. Bioenergetic role of halorhodopsin in *Halobacterium halobium* cells. *FEBS (Fed. Eur. Biochem. Soc.) Lett.* 131:341–345.

Weatherburn, C. E. 1961. A First Course in Mathematical Statistics. The English Language Book Society and Cambridge University Press, London.